REPORT DOCUMENTATION PAGE

Form Approved OMB NO. 0704-0188

1. REPORT DATE (DD-MM-YYYY)	2. REPORT TYPE	3. DATES COVERED (From - To)
	New Reprint	-

4. TITLE AND SUBTITLE
Pressure effects on the relaxation of an excited nitromethane molecule in an argon bath

5a. CONTRACT NUMBER
W911NF-09-1-0199

5b. GRANT NUMBER

5c. PROGRAM ELEMENT NUMBER
611102

6. AUTHORS
Luis A. Rivera-Rivera, Albert F. Wagner, Thomas D. Sewell, Donald L. Thompson

5d. PROJECT NUMBER

5e. TASK NUMBER

5f. WORK UNIT NUMBER

7. PERFORMING ORGANIZATION NAMES AND ADDRESSES
University of Missouri - Columbia
310 Jesse Hall

Columbia, MO 65211 -1230

8. PERFORMING ORGANIZATION REPORT NUMBER

9. SPONSORING/MONITORING AGENCY NAME(S) AND ADDRESS (ES)
U.S. Army Research Office
P.O. Box 12211
Research Triangle Park, NC 27709-2211

10. SPONSOR/MONITOR'S ACRONYM(S)
ARO

11. SPONSOR/MONITOR'S REPORT NUMBER(S)
56225-EG.5

12. DISTRIBUTION AVAILIBILITY STATEMENT
Approved for public release; distribution is unlimited.

13. SUPPLEMENTARY NOTES
The views, opinions and/or findings contained in this report are those of the author(s) and should not contrued as an official Department of the Army position, policy or decision, unless so designated by other documentation.

14. ABSTRACT
Classical molecular dynamics simulations were performed to study the relaxation of nitromethane in an Ar bath (of 1000 atoms) at 300 K and pressures 10, 50, 75, 100, 125, 150, 300, and 400 atm. The molecule was instantaneously excited by statistically distributing 50 kcal/mol among the internal degrees of freedom. At each pressure, 1000 trajectories were integrated for 1000 ps, except for 10 atm, for which the integration time was 5000 ps. The computed ensemble-averaged rotational energy decay is ?100 times faster than the vibrational energy decay. Both rotational and vibrational decay

15. SUBJECT TERMS
energy relaxation, pressure effects, nitromethane, classical trajectories

16. SECURITY CLASSIFICATION OF:			17. LIMITATION OF ABSTRACT	15. NUMBER OF PAGES	19a. NAME OF RESPONSIBLE PERSON
a. REPORT	b. ABSTRACT	c. THIS PAGE			Donald Thompson
UU	UU	UU	UU		19b. TELEPHONE NUMBER 573-882-0051

Report Title

Pressure effects on the relaxation of an excited nitromethane molecule in an argon bath

ABSTRACT

Classical molecular dynamics simulations were performed to study the relaxation of nitromethane in an Ar bath (of 1000 atoms) at 300 K and pressures 10, 50, 75, 100, 125, 150, 300, and 400 atm. The molecule was instantaneously excited by statistically distributing 50 kcal/mol among the internal degrees of freedom. At each pressure, 1000 trajectories were integrated for 1000 ps, except for 10 atm, for which the integration time was 5000 ps. The computed ensemble-averaged rotational energy decay is ?100 times faster than the vibrational energy decay. Both rotational and vibrational decay curves can be satisfactorily fit with the Lendvay-Schatz function, which involves two parameters: one for the initial rate and one for the curvature of the decay curve. The decay curves for all pressures exhibit positive curvature implying the rate slows as the molecule loses energy. The initial rotational relaxation rate is directly proportional to density over the interval of simulated densities, but the initial vibrational relaxation rate decreases with increasing density relative to the extrapolation of the limiting low-pressure proportionality to density. The initial vibrational relaxation rate and curvature are fit as functions of density. For the initial vibrational relaxation rate, the functional form of the fit arises from a combinatorial model for the frequency of nitromethane “simultaneously” colliding with multiple Ar atoms. Roll-off of the initial rate from its low-density extrapolation occurs because the cross section for collision events with L Ar atoms increases with L more slowly than L times the cross section for collision events with one Ar atom. The resulting density-dependent functions of the initial rate and curvature represent, reasonably well, all the vibrational decay curves except at the lowest density for which the functions overestimate the rate of decay. The decay over all gas phase densities is predicted by extrapolating the fits to condensed-phase densities.

REPORT DOCUMENTATION PAGE (SF298)
(Continuation Sheet)

Continuation for Block 13

ARO Report Number 56225.5-EG
Pressure effects on the relaxation of an excited ...

Block 13: Supplementary Note

Approved for public release; distribution is unlimited.

Pressure effects on the relaxation of an excited nitromethane molecule in an argon bath

Luis A. Rivera-Rivera,[1] Albert F. Wagner,[2] Thomas D. Sewell,[1] and Donald L. Thompson[1]
[1]*Department of Chemistry, University of Missouri-Columbia, Columbia, Missouri 65211-7600, USA*
[2]*Argonne National Laboratory, Chemical Sciences and Engineering Division, Argonne, Illinois 60439, USA*

(Received 30 September 2014; accepted 4 December 2014; published online 5 January 2015)

Classical molecular dynamics simulations were performed to study the relaxation of nitromethane in an Ar bath (of 1000 atoms) at 300 K and pressures 10, 50, 75, 100, 125, 150, 300, and 400 atm. The molecule was instantaneously excited by statistically distributing 50 kcal/mol among the internal degrees of freedom. At each pressure, 1000 trajectories were integrated for 1000 ps, except for 10 atm, for which the integration time was 5000 ps. The computed ensemble-averaged rotational energy decay is ∼100 times faster than the vibrational energy decay. Both rotational and vibrational decay curves can be satisfactorily fit with the Lendvay-Schatz function, which involves two parameters: one for the initial rate and one for the curvature of the decay curve. The decay curves for all pressures exhibit positive curvature implying the rate slows as the molecule loses energy. The initial rotational relaxation rate is directly proportional to density over the interval of simulated densities, but the initial vibrational relaxation rate decreases with increasing density relative to the extrapolation of the limiting low-pressure proportionality to density. The initial vibrational relaxation rate and curvature are fit as functions of density. For the initial vibrational relaxation rate, the functional form of the fit arises from a combinatorial model for the frequency of nitromethane "simultaneously" colliding with multiple Ar atoms. Roll-off of the initial rate from its low-density extrapolation occurs because the cross section for collision events with L Ar atoms increases with L more slowly than L times the cross section for collision events with one Ar atom. The resulting density-dependent functions of the initial rate and curvature represent, reasonably well, all the vibrational decay curves except at the lowest density for which the functions overestimate the rate of decay. The decay over all gas phase densities is predicted by extrapolating the fits to condensed-phase densities. © *2015 AIP Publishing LLC.* [http://dx.doi.org/10.1063/1.4904314]

I. INTRODUCTION

Advanced internal combustion engine designs[1] for efficient and clean combustion use dilute fuel mixtures at pressures considerably higher than currently employed. This strategy reduces peak combustion temperatures, leading to lower pollutant formation while retaining power density. Pressures as high as 500 bars are within the conceptual range of practical devices, far higher than typical peak operating conditions of 100 bars in current-generation engines. A rational design process requires knowledge of relaxation and reaction rates at higher pressures than are typically studied experimentally or theoretically. In particular, high pressure affects the unimolecular and recombination rates and branching ratios because relaxation and reaction processes compete to control the fate of highly excited molecule or radical.

Competition between relaxation and reaction occurs in many complex systems that do not involve combustion, such as the atmosphere. That competition is usually represented in models by the master equation (ME). There are a number of reviews[2–4] of ME applications to modeling combustion and atmospheric processes, and they generally emphasize that ME modeling is not reliably predictive stemming mainly from the lack of knowledge of energy transfer, angular momentum effects, and potential energy surfaces (PESs). This lack of knowledge concerns not only the absence of specific relaxation data on the many different, and often transient, species in complex systems but also the fact that the implementation of ME formulations in current models involves additional approximations.[5] More rigorous implementations of the ME approach are an active area of research[6] that will grow more challenging for higher pressures for which gas-molecule collisions are no longer isolated from one another. In order to provide species-specific relaxation data and to contribute to improved ME formulations, studies of collisional energy transfer over a wide interval of pressures are needed.

A number of techniques have been used to measure energy relaxation in highly excited molecules. These include infrared (IR) fluorescence detection,[7] high-resolution IR laser transient absorption spectroscopy,[8] time-resolved diode laser spectroscopy,[9] time-resolved ultraviolet absorption spectroscopy,[10] time-sliced velocity map ion imaging in molecular beams,[11] and laser-Schlieren[12] measurements. Most of the experimental measurements using these techniques have been carried out at low pressures for which a collision of the excited molecule with the buffer gas is rare and well isolated from any subsequent collisions of the excited molecule. However, several studies have been performed for higher pressures with the objective of relating the results to relaxation studies in liquids.[13] Of particular interest are the high-pressure

experimental studies[8(b),8(c),14,15] that have used supercritical fluids for which the density can be conveniently varied from small values typical of lower-pressure environments to large values that are only achieved at very high pressures.

Theoretical studies of collisional energy transfer involving highly excited molecules have been dominated by classical trajectory simulations. These are an alternative to rigorous quantum dynamics calculations, which are not feasible for systems of this size. Although the neglect of interference effects in classical mechanics affects its validity at low energies, quantum effects should be of minor importance for energy transfer at the high energies of interest here where the quantum-classical correspondence principle should be valid. The trajectory simulations can be logically divided into three groups. In the first group are simulations of ensembles of isolated collisions of bath gas species with a molecule or radical excited to a specific internal state. Simulation for a variety of initial states of the molecule produces results that can be fit to the probability transition matrix required by the ME formalism; examples can be found in Refs. 5 and 16–18. In the second group, the successive-collisions approximation of Lendvay and Schatz[19] is used in which IVR is assumed to randomize all but the conserved properties (total energy and angular momentum) in the post-collision state of a molecule prior to the next collision. No ME is involved, rather ensemble averages over independently generated sequences of successive collisions are used. At high enough pressures, the collision frequency will exceed the IVR rate and this approach will break down. In the third group, molecular dynamics (MD) simulations explicitly follow the motion of the excited molecule and all the bath gas species as they collide with each other and ultimately relax to a thermal distribution. This is by far the most expensive of the three groups of simulations because the vast majority of collisions are between bath gas species that serve only to sustain the bath gas thermal population. However, this approach is the only one that is equally valid at low and high pressures (up to and including the condensed phases of the bath). Because of the expense, such simulations are unusual, especially for highly excited molecules of greatest interest in combustion for which the time required for thermalization can be quite long. Several examples can be found in the work of Heidelbach *et al.*[20] for azulene/CO_2 and of Paul *et al.*[23] for the C_6F_6/N_2 system.

While it is impossible to briefly summarize the vast body of experimental and theoretical results on collisional energy transfer, there are two general observations of particular relevance to this paper. First, to the limits of experimental and theoretical resolutions, relaxation of initially highly excited molecules to thermal equilibrium is typically characterized by single-exponential decay. However, there are experimental[10,12] and theoretical[19,22,23] examples in the literature where multiple relaxation rates have been observed. Dove *et al.*[10] measured the collisional energy transfer of highly vibrationally excited CS_2 in 27 bath gases at 300 K. The energy-loss profiles are not exponential, including those for all the noble gases. Lendvay and Schatz[19] calculated the collisional energy relaxation of highly excited CS_2 in He and Xe at 300, 1000, and 2000 K. The relaxation of the molecule was found to be exponential in He but non-exponential in Xe. Kiefer *et al.*[12] reported shock-tube laser-Schlieren measurements of the high-temperature pyrolysis of ethane and CF_3CH_3 in which they observed two vibrational relaxation rates at temperatures above and below the onset of dissociation. Li and Thompson[22] calculated the vibrational relaxation of I_2 in Xe at ~300 K. At high initial energy and for an anharmonic I_2, the vibrational energy relaxation was found to be non-exponential. Paul *et al.*[23] calculated the relaxation of vibrationally excited C_6F_6 in N_2 bath at 298 K. For all pressures considered (35 atm–707 atm), the relaxation of the molecule was found to be non-exponential.

The second general observation is that while measurements and calculations of relaxation rates are directly proportional to pressure at pressures low enough for isolated gas-molecule collisions, the measurements of Schwarzer *et al.*[14] and the calculations of Heidelbach *et al.*[20,21] and Paul *et al.*[23] show that at high enough pressures, the relaxation rate grows more slowly than in direct proportion to the pressure. The Schwarzer *et al.* measurements of the relaxation of azulene in a variety of supercritical fluids including CO_2 show that a change in relaxation rate growth from direct proportional dependence to slower growth occurs at a density of ~1 mol/L or ~25 atm (estimated using the ideal gas law). A companion MD calculation by Heidelbach *et al.*[20] for azulene/CO_2 qualitatively reproduced both the measured low- and high-density relaxation rates, thus reproducing the departure of the rate from proportionality to pressure at high density. Finally, the MD simulations of Paul *et al.*[23] were carried out for a variation in pressure of over a factor of 20 and the computed relaxation rates show a less-than-proportional growth of the relaxation rate with pressure at high pressures.[24]

We report here the results of MD simulations of the relaxation of 50 kcal/mol of initial excitation in nitromethane (CH_3NO_2) in a 300 K Ar bath at eight different pressures from 10 atm to 400 atm. In these simulations, the molecule and all the Ar atoms are explicitly followed for at least 1000 ps, by which time the nitromethane has nearly reached thermal equilibrium. The 50 kcal/mol excitation is ~10 kcal/mol less than the weakest bond of the molecule, namely, the C–N linkage between the CH_3 and NO_2 groups.[25] Consequently, no dissociation occurs in the simulations. The pressure range of 10 atm–400 atm straddles the gas/supercritical-fluid transition. In the phase diagram of Ar, the critical point is at 150.68 K and 48.0 atm.[26] Consequently at 300 K, only pressures below 48 atm are in the gas phase. From 48 atm to 400 atm, Ar is a supercritical fluid. At more than an order of magnitude higher pressure, Ar exits the supercritical phase and condenses into a solid.

This is the first report among a planned series of reports on simulations designed to examine the relaxation of diatomic molecules, polyatomic molecules, and radical species in an Ar bath up to quite high pressures. The rest of this paper is organized as follows: Sec. II contains a discussion of computational methods including the PES used in the simulation. Section III contains a description of the results for both vibrational and rotational relaxations. The focus of Sec. IV is the discussion of a model that rationalizes the observed pressure dependence of the calculated vibrational relaxation rates. Section V contains conclusions and a discussion of several issues for which further work is needed to resolve.

II. COMPUTATIONAL METHODS

A. Potential energy surface

The nitromethane intramolecular potential was described by the Sorescu, Rice, and Thompson[25,27] (SRT) force field, which consists of a sum of Morse functions for the bond stretches, harmonic oscillators for bond angles, and cosine series for the HCNO dihedral angles and the improper dihedral angle for the C–NO_2 out-of-plane deformation. Nitromethane-Ar and Ar-Ar interactions were described by the Buckingham potential

$$V_{\alpha\beta} = A_{\alpha\beta} e^{-\frac{R}{B_{\alpha\beta}}} - \frac{C_{\alpha\beta}}{R^6}, \tag{1}$$

where R is the distance between atoms α and β. The values of the Ar-Ar parameters, $A_{\text{Ar-Ar}} = 695{,}963.0$ kcal/mol, $B_{\text{Ar–}Ar} = 0.24748$ Å, and $C_{\text{Ar–}Ar} = 1294.81$ Å^6 kcal/mol, were obtained by fitting the Colbourn and Douglas[28] potential to Eq. (1). The Colbourn and Douglas potential, which is given at discrete R values, is based on spectroscopic data for the five lowest vibrational states of Ar_2, with corrections for long-range forces based on fitting to the experimental second virial coefficient. Relative one-standard deviation uncertainties in the fitted parameters are ±10%, ±1%, and ±1% for $A_{\text{Ar-Ar}}$, $B_{\text{Ar-Ar}}$, and $C_{\text{Ar-Ar}}$, respectively. The parameters for the nitromethane-Ar interactions were obtained using the combination rules

$$\begin{aligned} A_{\alpha\beta} &= \sqrt{A_{\alpha\alpha} A_{\beta\beta}}, \\ B_{\alpha\beta} &= \left(B_{\alpha\alpha} + B_{\beta\beta}\right)/2, \\ C_{\alpha\beta} &= \sqrt{C_{\alpha\alpha} C_{\beta\beta}}, \end{aligned} \tag{2}$$

where α is Ar and β is C, N, O, or H. The values of the homo-atom parameters $A_{\beta\beta}$, $B_{\beta\beta}$, and $C_{\beta\beta}$ for the C-C, N-N, O-O, and H-H interactions were taken from Sorescu *et al.*[29]

The SRT nitromethane force field produces harmonic frequencies in good accord with *ab initio* calculations.[25] These frequencies yield an harmonic zero point energy of 30.3 kcal/mol, comparable to the classical internal energy of 50 kcal/mol at the start of the trajectories studied here. However, this zero point energy is not available for transfer to the bath gas and for this reason is excluded from the trajectory calculations. The harmonic frequencies also permit an estimation of the quantum dynamical vibrational density of states using the Whitten Rabinovitch approximation.[30] By this estimate, the number of harmonic vibrational states per wavenumber varied from ~500 to 300,000 over the internal vibrational energy range of 20.0 kcal/mole to 45.0 kcal/mol typically sampled by our classical trajectories. With such a large density of states, quantum effects should not be prominent over this range of energies. At much lower vibrational energies, quantum effects can become more important. As an example, at 300 K, the 15 vibrational degrees of freedom of nitromethane should lead to a thermal vibrational energy of 8.94 kcal/mol, that is, 15 kT where k is the Boltzmann constant. However, the quantum harmonic energy above the zero point energy for nitromethane is only 1.00 kcal/mol.[31] In effect, the vibrational quantum of most of the degrees of freedom is much larger than kT, leading to a quantized form of nitromethane that behaves as if it is a classical molecule with much fewer degrees of freedom. Our classical trajectory study follows in the tradition of many published trajectory studies of relaxation, avoids the tail end of vibrational relaxation where quantum effects can become more important, and should provide a useful description of relaxation processes in nitromethane.

B. Simulations

Initial conditions for the relaxation simulations were obtained in four steps: (1) determination of the equilibrium volumes at 300 K for the eight pressures studied, (2) selection of microcanonical phase space points for the internal degrees of freedom of the excited molecule, (3) equilibration of the Ar bath around the molecule, with the molecule held rigid and stationary during equilibration, and (4) assignment of thermal translational velocities to the molecule.

All simulations with the bath gas were performed using the LAMMPS[32] code, with three-dimensional periodic boundary conditions for a simulation box with initial dimensions of 60.0 Å × 60.0 Å × 60.0 Å containing one molecule and 1000 Ar atoms. The starting geometry of the molecule corresponds to the SRT equilibrium geometry and the center of mass of the molecule was initially placed at the center of the box, that is, at $X = Y = Z = 30.0$ Å. The initial positions of the Ar atoms were chosen randomly as

$$\begin{aligned} X &= \xi_x L, \\ Y &= \xi_y L, \\ Z &= \xi_z L, \end{aligned} \tag{3}$$

where ξ_i ($i = X, Y, Z$) is a pseudorandom number uniformly distributed on (0,1) and L is the initial edge length of the cubic simulation cell. If the distance of the kth Ar atom from an atom of the nitromethane molecule or any of the $k-1$ Ar atoms already in the simulation cell was less than 1.0 Å, then a new position was chosen (the Buckingham potential of Eq. (1) passes through a maximum at unrealistically small values of R [ranging from 0.69 Å to 0.77 Å for the Ar-Ar, Ar-C, Ar-N, Ar-O, and Ar-H pairs used here] then diverges to negative infinity, necessitating the 1.0 Å exclusion test). Starting from these system configurations 200 ps isobaric-isothermal (*NPT*) simulations were run at $T = 300$ K and $P = 10, 50, 75, 100, 125, 150, 300$, and 400 atm using a 0.10 fs time step, barostat and thermostat coupling parameters 10.0 fs and 100.0 fs, respectively, and a simulation box constrained to remain cubic. Initial velocities for all Ar and nitromethane atoms were selected from the Maxwell distribution. The last 100 ps of the *NPT* simulation were used to calculate the average length of the simulation cell edge used for each pressure, $\langle L \rangle = 159.75781$ Å for 10 atm, 92.84972 Å for 50 atm, 80.86864 Å for 75 atm, 73.24327 Å for 100 atm, 67.96773 Å for 125 atm, 63.87542 Å for 150 atm, 51.41449 Å for 300 atm, and 47.77249 Å for 400 atm. These edge lengths were used to define the volumes of the cells for all subsequent isochoric-isothermal (*NVT*) and isochoric-isoergic (*NVE*) simulations.

Microcanonical phase space points for the isolated excited molecule were obtained using the GENDYN[33] code. Starting with the molecule at the SRT equilibrium geometry, a Markov

walk[34] of two-million steps was carried out in configuration space to move the system away from equilibrium to a random geometry consistent with the microcanonical ensemble for the internal degrees of freedom with no restriction on the angular momentum. At each Markov step, each of the 21 Cartesian coordinates was displaced by random fractions of ±0.055 Å subject to the restriction that none of the six covalent bond lengths in the molecule became larger than 2.0 Å; these parameters gave an acceptance/rejection ratio of 0.48 for the molecular internal energy studied (50.0 kcal/mol). The initial phase space point for the internal degrees of freedom of the excited molecule for the first *NVE* relaxation trajectory was obtained by combining the configuration at the end of the initial random walk with a set of 21 Cartesian momenta selected from the mass-weighted normal distribution with zero mean and unit variance, removing the center-of-mass momentum, and scaling the atomic momenta to give the desired microcanonical energy. Molecular initial conditions for subsequent trajectories were similarly obtained based on configurations sampled at regular 10 000 step intervals along the Markov chain.

Following the selection for the initial conditions for the molecule, the molecular center of mass was located at the center of the simulation box with edge length $\langle L(P)\rangle$. Then, the molecule was held fixed and rigid as new positions of all Ar atoms were chosen randomly using Eq. (3) with $L = \langle L(P)\rangle$ and new velocities for the Ar atoms were selected from the Maxwell distribution. Nosé-Hoover[35] *NVT* simulations of 100 ps duration were performed at $T = 300$ K with time step 0.10 fs and thermostat coupling parameter 10.0 fs. After the thermalization of the bath, the internal velocities of the molecule were restored and thermal velocities for the molecular center of mass were selected from the Maxwell distribution at 300 K. This completes the description of the initial conditions selection.

Trajectories were calculated in the *NVE* ensemble, with fixed time step 0.05 fs, to determine the relaxation rates. Tests were performed for $P = 100$ atm for systems containing 500, 1000, and 1500 Ar atoms. It was found that the decay of the excess vibrational energy of the molecule was converged with 1000 Ar atoms. Ensembles of 1000 trajectories were computed for each pressure. Each trajectory was integrated for 1000 ps, except for 10 atm for which the trajectories were integrated for 5000 ps.

Translational, vibrational, and rotational energies of the nitromethane molecule were calculated as functions of time. The separation between vibrational and rotational energies of the molecule at a given time was approximated as follows: After removing the instantaneous center-of-mass velocity and position, the internal energy of the molecule was defined as the sum of the intramolecular potential energy and the remaining kinetic energy. The vibrational energy was defined as the energy of the molecule that remained after subtracting the molecular angular momentum, and the rotational energy was defined as the difference between the internal energy and the vibrational energy.

As mentioned above, at pressures greater than 48 atm, Ar is a supercritical fluid. To our knowledge, MD calculations have not been performed with the potential used here to model Ar in the supercritical regime. However, a quite similar pairwise additive *ab initio* Ar-Ar potential[36] has been used in MD calculations[37] of 500 Ar atoms with periodic boundary conditions at a temperature of 350 K and a pressure range of ~50 atm to ~900 atm. The calculated atomic pair correlation function agreed well with the experimental one measured by neutron diffraction.[34] This suggests that the simulations reported here appropriately describe the supercritical regime.

III. RESULTS AND DISCUSSION

We have calculated trajectories to determine the relaxation of nitromethane, with initial internal energy 50.0 kcal/mol above the classical ground state, in Ar at 300 K and at pressures of 10, 50, 75, 100, 125, 150, 300, and 400 atm. In the first part of this section, the ensemble-averaged energy in nitromethane as a function of time is presented for all eight pressures, and the qualitative features of the decay rates are discussed. In the second part of this section, analytic fits to the decay curves are presented, which allows for a more precise and quantitative discussion of these features.

A. Decay curves

The ensemble-averaged rotational (blue curve), vibrational (red curve), and translational (green curve) energies over 1000 ps are shown in Fig. 1 for 100 atm. The results clearly show the equilibration of the rotational and translational energy to values approaching 1.5 kT (~0.9 kcal/mol

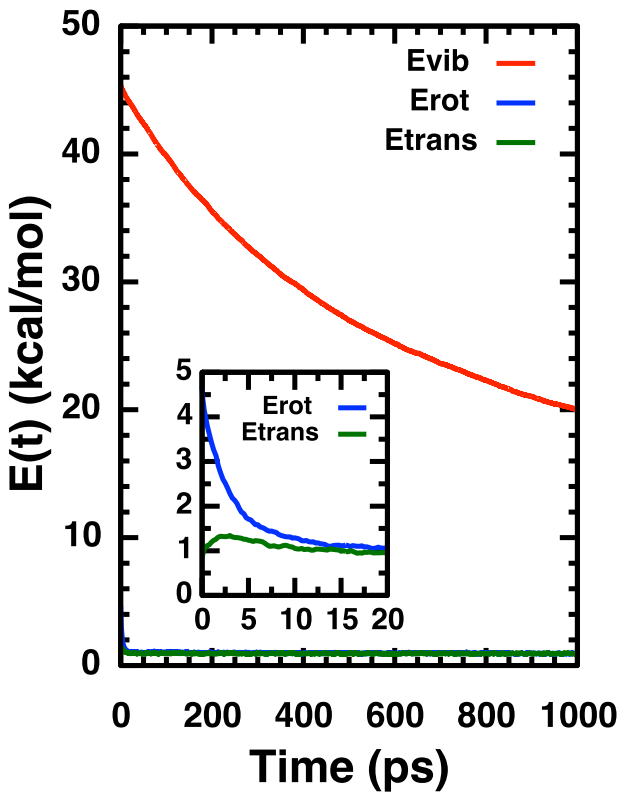

FIG. 1. Ensemble-averaged vibrational, rotational, and translational energies versus time at 100 atm. The inset is a zoom-in of the lower left-hand corner of the plot.

for $T = 300$ K). The inset in Fig. 1 shows that rotation and translation are equilibrated within ~15 ps, while the full plot shows that the vibrational energy does not reach equilibrium within 1000 ps. These equilibration times vary with pressure in expected ways but the two-orders-of-magnitude difference in equilibration times for rotation and vibration stays the same. As the green curve in the inset in Fig. 1 shows, the translational energy of the molecule deviates slightly from the equilibrium value for the first few picoseconds. This is an artifact of the initial conditions selection: Interactions between the molecule and the bath were neglected during assignment of the molecular center-of-mass kinetic energy whereas, in reality, the forces between the molecule and the gas atoms in the starting configuration will not generally be precisely zero.

In Fig. 2, the normalized ensemble-averaged *excess* vibrational energy $E_{nrm\text{-}vib}(t)$ is plotted as a function of time for all eight pressures in the main panel for $t \leq 1000$ ps and for $P = 10$ atm in the inset for $t \leq 5000$ ps. Excess energy at a given time is the energy above the thermal energy at that time including the temperature increase of the bath gas due to molecular energy lost up to that time (with full thermalization of the initial molecular excitation of 50 kcal/mol over 1000 Ar atoms, the temperature increase is ~13 K). The results are normalized to the excess energy appropriate to the initial absolute value of the energy shown in Fig. 1, which is the same in all cases. The excess vibrational energy is plotted on a log scale, for which single-exponential decay would be linear (because the asymptotic value of the excess energy is zero). The results show curvature at the higher pressures indicating multiple decay rates over the temporal interval of the plot. For the lowest pressure, 10 atm, it appears that a single decay rate applies over 1000 ps; however, as the results in the inset show, when the process is followed for 5000 ps, there is clearly a curvature. The results in Fig. 2 show that there is not a single decay rate at any pressure as the vibrational energy relaxes to equilibrium. The results in Fig. 2 also clearly show that the excess vibrational energy decays at increasing rates with increasing pressure.

It is useful to examine the behavior of the rotational relaxation on a much shorter time scale than shown in Fig. 2 for vibrational relaxation. The results shown in Fig. 3 are for the excess rotational energy $E_{nrm\text{-}rot}(t)$ for the first 50 ps except for 10 atm, which is shown for 200 ps (see inset). The most important feature of Fig. 3 is that, as was the case for the vibrational relaxation shown in Fig. 2, excess rotational energy decays with a rate that increases monotonically with pressure. However, the most striking feature of the results in Fig. 3 is that approximately 5% of the initial excess rotational energy remains in the molecule. Although not shown in the figure, at 1000 ps, some of this 5% of the initial rotational energy still remains. As seen in the inset of Fig. 1, 5% of the initial rotational energy amounts to a couple of tenths of a kcal/mol. Some of this residual excess energy could be due to the approximate nature of separation of rotational and vibrational energies. Also, the statistical variations due to finite sample size are comparable to this slow decay feature as seen

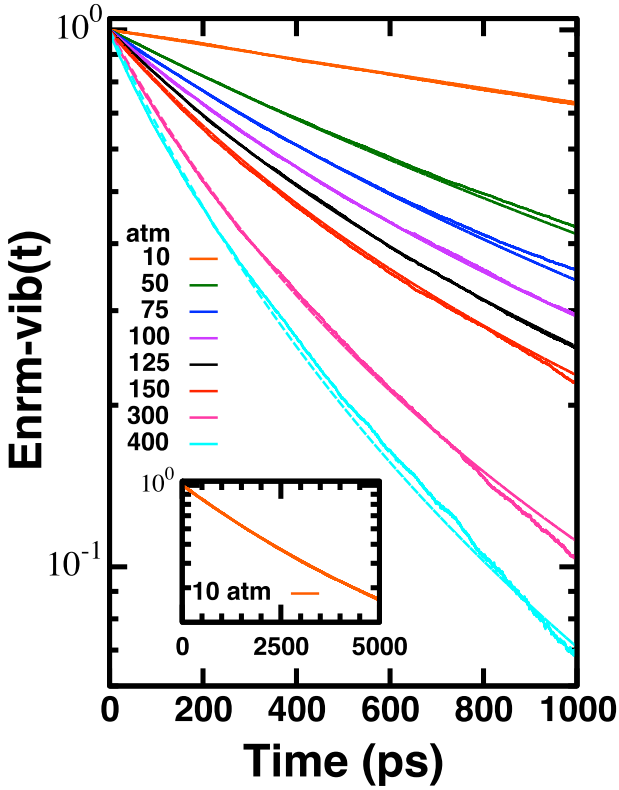

FIG. 2. $E_{nrm\text{-}vib}$ versus time. The solid curves are the trajectory results and the dashed curves are fits to the trajectory results. The inset is an expansion of the 10 atm results to 5000 ps.

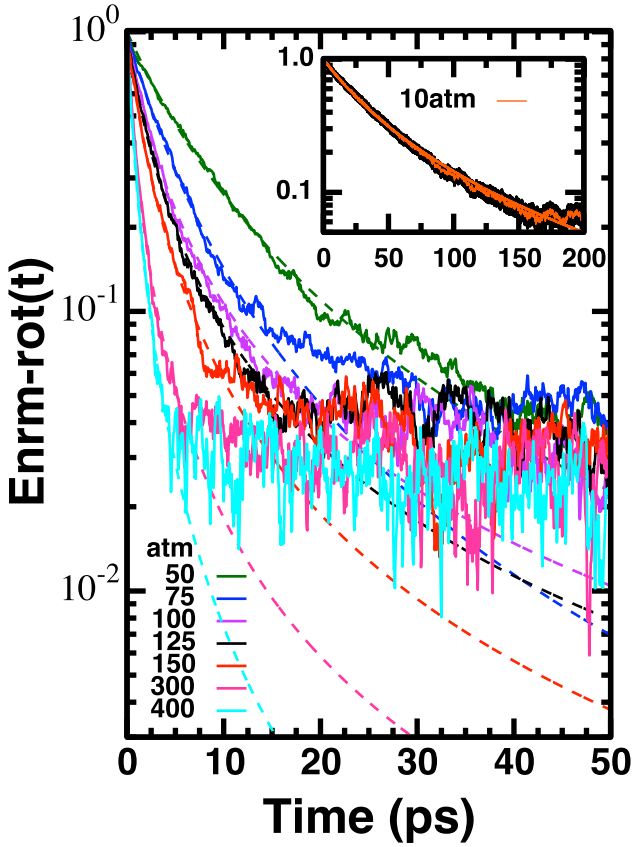

FIG. 3. $E_{nrm\text{-}rot}$ versus time analogous to Fig. 2 only for a maximum time of 50 ps (200 ps for the inset). Black shading in the inset is the statistical uncertainty.

in the black shading in the inset, which represents one-σ statistical error in the mean for 10 atm (σ values at other pressures are similar). Finite sampling statistics also affect the value of excess rotational energy through statistical variations in the rising temperature of the bath gas. To understand more about this slowly decaying residual of rotational energy, the ensemble size would need to be significantly larger, an effort that has not been undertaken for this paper.

B. Analytic fits to decay curves

The presence of curvature in Fig. 2 for the excess vibrational energy requires a representation more flexible than a single exponential. For example, Paul *et al.*[23] used a bi-exponential fit to represent curvature in their C_6F_6/N_2 results. While this form can fit our data reasonably well, it has two disadvantages. First, if one requires the two coefficients, one for each exponential, to sum to the initial value of the energy, there are three adjustable parameters. For some of the data in Fig. 2, there are strong correlations between the three parameters, leading to large uncertainties in the three optimized values. Second, the two decay rates in some cases are not sufficiently different for one rate to completely dominate in some portion of the temporal interval of Figs. 2 and 3, which complicates separate interpretations of each rate. Another way to say this is that there is no physical motivation for *just* two rates. Rather, the decay rate is continuously changing as the energy of the molecule transfers to the bath gas and the fits do not capture this with just two rates.

An alternative function was introduced by Lendvay and Schatz[19] (LS) who integrated out the often used relationship $\Delta E \propto E(t)^m$ from isolated-molecule/bath-gas collision studies, where ΔE is the average energy lost per collision by the molecule with initial energy $E(t)$. Because the ΔE is proportional to the derivative of $E(t)$, $\Delta E \propto E(t)^m$ can be converted into a differential equation whose integration gives

$$\frac{E(t)}{E(0)} \equiv E_{nrm}(t) = [1-(1-m)k_i t]^{\frac{1}{1-m}}. \quad (4)$$

This form for the decay of the normalized energy $E_{nrm}(t)$ has the virtue that it involves only *two* parameters, not three, and each parameter more clearly responds to different temporal regions of the decay. At $t = 0$, the k_i parameter equals dE_{nrm}/dt, the initial rate of decay. To the extent that this form is appropriate, k_i will be determined primarily by the early behavior of the decay curve. The parameter m determines curvature. When $m = 1$, Eq. (4) can be shown[38] to collapse to a single exponential function with rate k_i. For $m > 1$, $E_{nrm}(t)$ curves up from the single-exponential straight-line behavior on a semi-log plot, meaning that as energy flows out of the molecule, the rate of loss of the remaining energy slows down. For $m < 1$ (including negative values), $E_{nrm}(t)$ curves down from single-exponential (linear) behavior, meaning that as energy flows out of the molecule, the rate of loss of the remaining energy accelerates. While $m < 1$ can result in an optimal fit of Eq. (4) to ensemble-averaged energy decay over a finite interval of time, it is not physically meaningful because the term inside the brackets in Eq. (4) will become negative at large values of time, producing an $E_{nrm}(t)$ that is no longer a real number. Because Eq. (4) cannot be derived from more rigorous collision theory, the expression is only a fitting function, however, one with only two parameters, each of which has a useful phenomenological interpretation.

The application of the LS fit for excess vibrational energy decay is represented as dashed curves in Fig. 2. The optimal parameter values for m and k_i are listed in Table I along with the rms absolute error for the normalized decay $E_{nrm\text{-vib}}(t)$. Also listed are the uncertainties Δm and Δk_i determined by a bootstrap method[39] using 2000 random realizations of the 1000 trajectories calculated at a given pressure. For all pressures, the fit has an rms error less than 0.01. Inspection of Fig. 2 shows that while the fit is quite good for each pressure, at higher pressures the computed $E_{nrm\text{-vib}}(t)$ becomes more ragged at longer times. This raggedness is probably due to the finite sampling error becoming comparable to the quite small excess vibrational energies at these long times. Although it is not apparent at the scale of Fig. 2, the LS fit for the 10 atm results is somewhat inaccurate at early times; this is not typical of the fits at other nearby pressures. Figure 4 is a zoom-in of the first 400 ps of Fig. 2 for the five lowest pressures. Unlike the results at all the other pressures, $E_{nrm\text{-vib}}(t)$ at 10 atm initially curves *downward*. This would require a value of m less than 1 but the inset in Fig. 2 shows clearly that over 5000 ps $E_{nrm\text{-vib}}(t)$ does substantially curve upward, leading to least-squares value $m = 1.34$ (see Table I). Figure 5 shows plots of the values of m and k_i as functions of the time interval of the 10 atm data included in the fit, always starting from $t = 0$. Clearly, LS fits confined to early times have values of $m < 1$ and k_i values ~80% of the values listed in Table I. The implication of this is that the least-squares value of k_i for 10 atm (see Table I) should

TABLE I. As functions of pressure and density, parameter values m and k_i for vibrational relaxation, their uncertainties Δm and Δk_i, and the rms fitting error for the LS fit to $E_{nrm\text{-vib}}(t)$.

Pressure (atm)	Density ($\times 10^3$ Å^{-3})	m	Δm	k_i ($\times 10^3$ ps^{-1})	Δk_i ($\times 10^5$ ps^{-1})	rms error ($\times 10^3$)
10	0.245	1.34	0.004	0.341	0.09	3.11
50	1.25	1.46	0.045	1.04	1.92	1.25
75	1.89	1.58	0.037	1.43	2.58	1.89
100	2.55	1.56	0.031	1.75	2.96	2.55
125	3.19	1.53	0.027	2.00	3.09	3.18
150	3.84	1.60	0.024	2.41	3.69	3.84
300	7.36	1.42	0.018	3.68	5.38	7.36
400	9.17	1.37	0.018	4.40	6.54	9.17

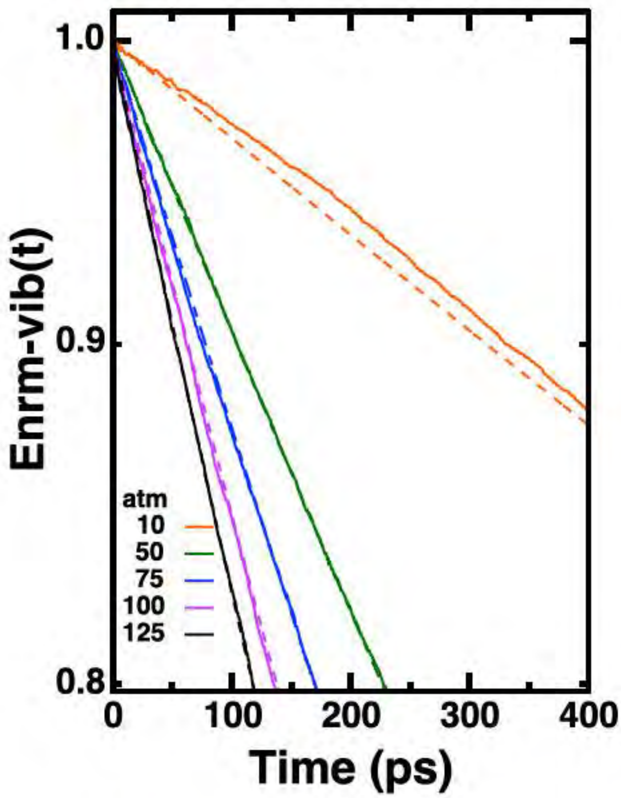

FIG. 4. As in Fig. 2, except a zoom-in of the first 400 ps and only for the five lowest pressures.

be interpreted as a more global value of the rate rather than the actual initial relaxation rate, which (see Fig. 5) is noticeably slower. As Fig. 4 shows, this difficulty is unique to the 10 atm results and may represent some small-scale imperfections in the preparation of the initial conditions of the simulation. This warrants further study.

At lower pressures corresponding more closely to ideal behavior, the density and pressure are directly proportional to each other; however, at higher pressures, the density more slowly increases in response to pressure. The first noticeable break in direct proportionality can be seen in the last few rows of Table I. Extreme pressures are necessary to condense the Ar gas to the solid state at 300 K, but it is instructive to investigate how much the density for the highest value studied here (see Table I) differs from the nominal solid-state density. Using the Ar-Ar potential described in Sec. II A, the Ar hard-sphere radius is 1.675 Å. Given that radius as the spherical size of Ar, the packed-sphere formula[40] of Gauss provides the maximum number of spheres that can be packed into a given volume. That density is 0.0374 $Å^{-3}$. This value can be compared to the measured[41] density of 0.0275 $Å^{-3}$ for face-centered-cubic crystal Ar at 4.2 K and saturated vapor pressure. The crystal structure expands with increasing temperature and contracts with increasing pressure[42] for an unknown end result at 300 K and many thousands of atmospheres of pressure. Most likely, the packed-sphere density 0.0374 $Å^{-3}$ is an upper bound for the true density of the solid phase of Ar at 300 K and by that guide the maximum density studied here is ~25% of the solid-state density.

Plots of the parameter values m and k_i as functions of density are shown, respectively, in Figs. 6 and 7. The results in Fig. 6 show that the m parameter assumes values in a narrow range of 1.3–1.6 over a factor of ~40 variation in the density.

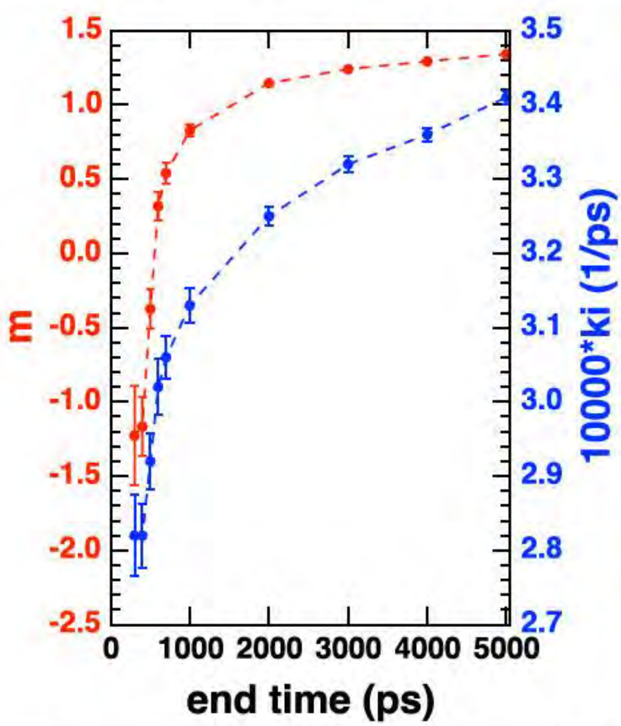

FIG. 5. Optimized values of m and k_i for vibrational relaxation at 10 atm plotted versus the time interval of the $E_{nrm\text{-}vib}$ data. Parameters are color coded to the appropriate axis. Dashed lines are straight line segments to aid the eye.

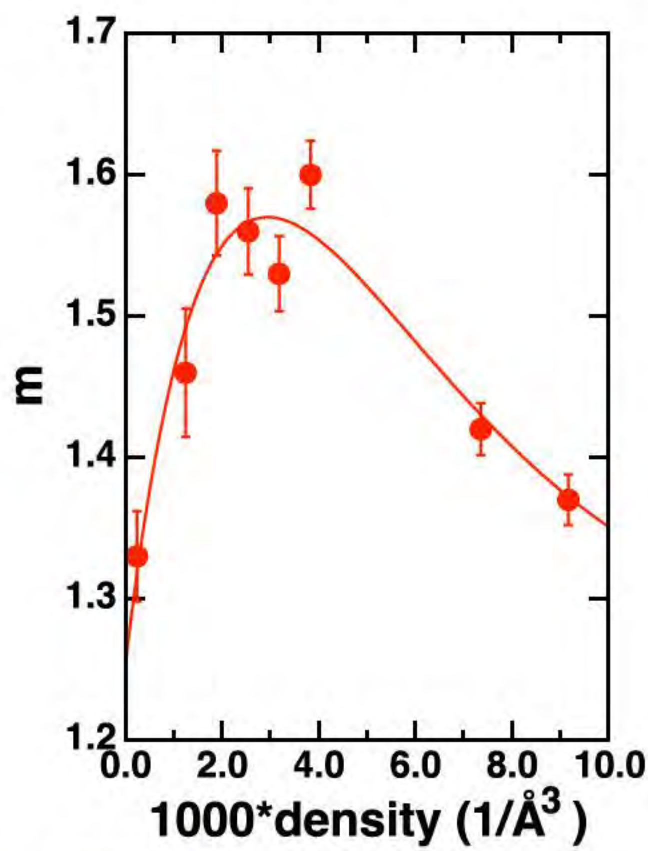

FIG. 6. From Table I, m values for vibrational relaxation with their uncertainty Δm versus density. The solid curve is a fit (see text for details).

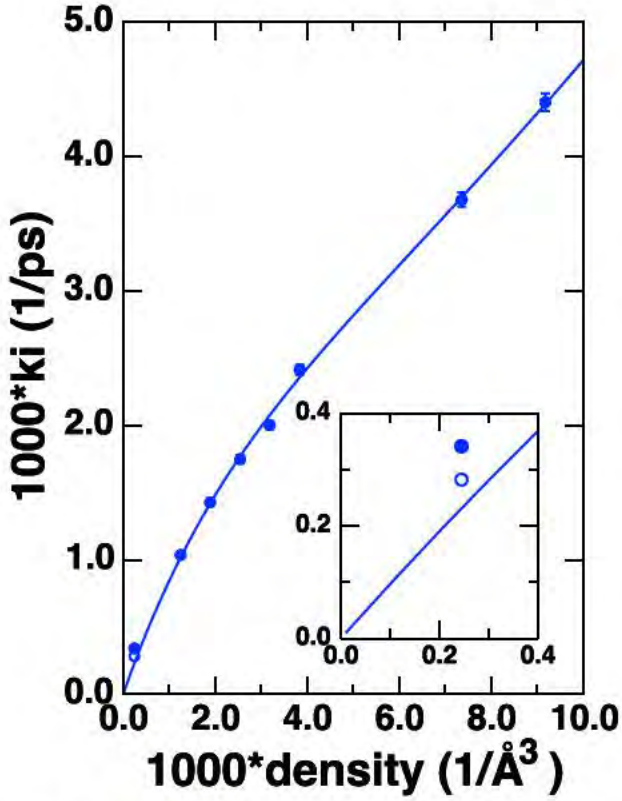

FIG. 7. From Table I, k_i values for vibrational relaxation with their uncertainty Δk_i versus density. The solid curve is a fit (see text for details). The single open circle is the early time value of k_i, taken from Fig. 5.

The persistence of this band of curvature over such a wide variation of conditions suggests that the unchanging internal structure of nitromethane is involved. Perhaps the effective coupling of high- to low-frequency vibrational modes changes in the molecule as energy is lost, or perhaps the degree of coupling of vibrational and rotational energies changes with energy loss. Such changes could influence how readily the molecular internal energy is lost to the bath and result in a slowdown of the rate as the energy decreases. Additional studies to uncover the mechanisms responsible for curvature are planned. The C_6F_6/Ar study of Paul *et al.*[23] also exhibits curvature (although not characterized by a parameter m) at all pressures studied.

The solid curve in Fig. 6 is a fit of the density dependence of m to the functional form $a + b\rho e^{-c\rho}$, where ρ is the density. Because the mechanisms of curvature are not yet known, this functional form is one of convenience and is not based on any physical justifications. For the least-squares parameter values $(a,b,c) = (1.252, 292.7\text{Å}^3, 338.8\text{Å}^3)$, this functional form represents the results within a two-sigma uncertainty with Δm in Table I being sigma. The least-squares value of a suggests that substantial curvature exists for all gas-phase densities.

The results in Fig. 7 show that the k_i parameter assumes values that increase monotonically over the factor of ~40 variation in the density. However, the results in the figure also clearly show that k_i is not directly proportional to density over this interval. At the density of ~0.002 Å^{-3}, corresponding to ~100 atm, k_i begins to drop below what is expected from a direct proportionality. Recall that k_i is the relaxation rate at $t = 0$ for the LS fit. The initial conditions of the molecule are statistically identical for all densities (ignoring the small artifact noted for the translational energy in the discussion of Fig. 1). This implies that the loss of direct proportionality is a consequence of a change in the nature of the interaction of Ar bath with the molecule as a function of density. A proposed mechanism for this change, described in Sec. IV, leads to a functional form whose least-squares optimization leads to the solid curve in Fig. 7.

The LS fits for excess rotational energy decay are shown by dashed curves in Fig. 3. However, the presence of the slowly decaying residual energy makes this fitting not straightforward. Fitting rotational decay over the full 1000 ps of the simulation sacrifices an accurate representation of the major early decay for a more reliable representation of the minor residual decay. Given that the mechanism of the residual decay is not known, a physically motivated functional form different from and more flexible than LS cannot now be developed. Rather, the approach taken for the results in Fig. 3 is to limit at each pressure the temporal interval over which the LS fit is applied. The error of the mean due to finite sampling is available at each value of $E_{nrm\text{-rot}}(t)$ for each pressure in Fig. 3 (see the black shading in the inset), and the limit selected is the maximum time for which the LS fit falls within this error 85% of the time. Obviously 85% is not physically motivated. A higher percentage results in a fit over a shorter span that leaves out some of the major decay. A lower percentage results in a compromised fit that includes the residual tail. Inspection of Fig. 3 reveals that the final LS fit represents the major decay well with the possible exception of $E_{\text{nrm-rot}}(t)$ at 75 atm, which exhibits a more gradual approach to the residual tail than do the results at nearby pressures.

Analogous to Table I, the optimal parameter values for m and k_i are listed in Table II along with the rms absolute error for the normalized decay $E_{nrm\text{-rot}}(t)$ and the maximum time over which the fit was applied. The fitting error is ~2 to ~35 times larger than that for $E_{nrm\text{-vib}}(t)$ and for a temporal interval that is 0.005–5 times smaller. This is obviously a reflection of the noisier data in Fig. 3 due to the relatively small magnitude of $E_{nrm\text{-rot}}(t)$ compared to $E_{nrm\text{-vib}}(t)$. The maximum time over which the LS fit is applied increases monotonically with pressure except for 75 atm for which the approach of the major decay to the residual decay is noticeably slower. Because of the less-than-definitive nature of the fit, no attempt was made to determine the uncertainties Δm and Δk_i. However, it is quite clear that the m value for rotational relaxation (Table II) is consistent with the 1.3–1.6 range for vibrational relaxation (Table I). The k_i value for rotational relaxation (Table II) is at least a hundred times larger than the corresponding value for vibrational relaxation (Table I).

A two-sided plot of both the m and k_i parameter values for rotational relaxation from Table II as functions of density is shown in Fig. 8. As with the vibrational m dependence, the rotational m dependence on density in Fig. 8 is relatively small at the low end and high end of the density interval studied and exhibits a maximum for intermediate density values. Unlike the vibrational k_i dependence (Fig. 7), the k_i dependence on density in Fig. 8 is directly proportional to density as indicated by the least-squares straight line with a zero intercept.

TABLE II. As a function of pressure and density, parameter values m and k_i for rotational relaxation, the rms fitting error, and the maximum time for the LS fit to $E_{nrm\text{-}rot}(t)$.

Pressure (atm)	Density ($\times 10^{-3}$Å^{-3})	m	k_i (ps^{-1})	rms error ($\times 10^{-2}$)	Max time (ps)
10	0.245	1.42	0.030	0.87	195.4
50	1.249	1.40	0.177	1.23	27.8
75	1.891	1.37	0.286	1.28	14.0
100	2.545	1.59	0.466	1.04	21.8
125	3.185	1.58	0.537	0.92	19.4
150	3.837	1.52	0.663	1.13	7.9
300	7.358	1.56	1.50	0.88	7.0
400	9.172	1.43	1.68	1.31	4.9

This qualitative difference between vibrational and rotational dynamics is discussed in Sec. IV.

IV. A PROPOSED MODEL

In Figs. 6 and 7, $E_{nrm\text{-}vib}(t)$ has been characterized in terms of k_i and m. The m parameter represents the curvature over the entire temporal interval of the simulations and undoubtedly involves the internal coupling of modes of motion in nitromethane as the internal energy decreases as well as the changing character of nitromethane/Ar interactions for different densities. The curve in Fig. 6 is the density dependence fit to a convenient functional form unmotivated by any insight into the molecular mechanisms responsible for curvature. In contrast, the k_i parameter is nominally the initial rate of decay of $E_{nrm\text{-}vib}(t)$. Because the initial conditions of the molecule are statistically the same at every pressure, the pressure dependence of k_i is primarily dependent on the changes in the nitromethane/Ar interactions as a function of density. In this section, a physical model will be developed for the density dependence of the nitromethane/Ar interactions that motivates the functional form used to obtain the fit to the k_i pressure dependence shown in Fig. 7.

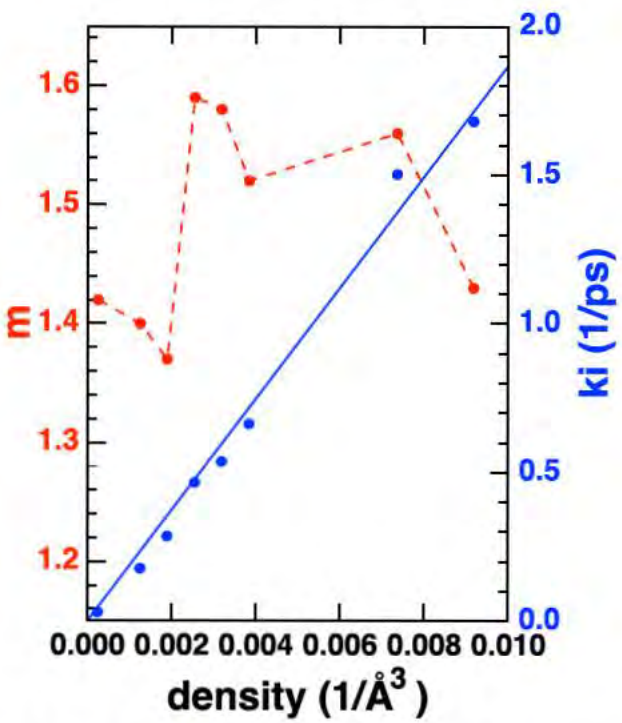

FIG. 8. From Table II, m and k_i values for rotational relaxation versus density. The dashed line segments connect m values. The solid line is a direct proportionality fit to k_i.

At low densities for which the isolated binary collision assumption is valid, k_i should be directly proportional to density. As the density increases, one obvious possible change is the development of Ar clusters. If the clusters are numerous enough, and if the vibrational relaxation efficacy of a nitromethane/Ar$_n$ collision is sufficiently different from that of a nitromethane/Ar-atom collision, the loss of linear proportionality between k_i and density seen in Fig. 7 could be explained. A simple test of this hypothesis is to run the simulation without any van der Waals wells. To this end, simulations at 10 atm and 150 atm[43] were performed in which all Ar-Ar and nitromethane-Ar pairwise Buckingham potentials, Eq. (1), were truncated at the bottom of each well and shifted vertically such that the energy at and beyond the truncation point is zero. This means that all interactions of Ar with itself or nitromethane are purely repulsive and therefore no Ar clusters or Ar-molecule complexes can be formed. The resulting $E_{nrm\text{-}vib}(t)$ was fit to the LS function and yielded k_i values that are 49% (for 10 atm) and 47% (for 150 atm) as large as the corresponding values shown in Table I. The fact that these two percentages are so close in value indicates that the *scale* of the functional dependence on pressure has changed but the *shape* has not. This means that in the absence of van der Waals clusters of any sort, k_i still departs from proportionality to density at higher densities. The fact that k_i is smaller in the absence of potential wells is generally consistent with the physical notion[44] that wells increase the relative velocity of the collision just prior to contact with the repulsive wall of the molecule.

The cluster hypothesis can be regarded as a restricted form of a more general model wherein increasing density results in the molecule interacting simultaneously with multiple Ar atoms. At condensed-phase densities, the molecule would be in contact with Ar atoms over its entire surface area. As discussed in Sec. III, at 400 atm (the highest pressure studied) the density is about 25% of the nominal solid-state density. Of course, at low enough densities, nitromethane will only interact with one, if any, Ar atom at a given time. As the density is increased, the probability of a nitromethane collision event involving two or more Ar atoms simultaneously increases. If the per-collision efficacy of $E_{nrm\text{-}vib}(t)$ relaxation varies with the number of Ar atoms in a single collision event, then the loss of direct propor-

tionality of k_i seen in Fig. 7 could be explained. Note that this explanation depends on multiple, simultaneous molecule/bath-gas interactions due to high-density proximity. As such it is consistent with bound interactions as in clusters and complexes but does not *require* that the interactions be bound.

If one approximates both Ar and nitromethane as hard spheres, one can render the notional model outlined above into an exercise in combinatorial arithmetic. Imagine placing the nitromethane hard sphere at the center of a large but finite volume and discretizing all of the volume outside of nitromethane into cells that can hold at most one Ar hard sphere. Figure 9 is a two-dimensional illustration of this model. There will be a finite number of cells that are adjacent to the nitromethane (as indicated by the white squares in Fig. 9) but the vast majority of the cells do not border nitromethane (yellow squares in Fig. 9). A given simulation density sets how many Ar atoms must go into the finite volume to be consistent with that density. Because of the hard-sphere approximation, any cell in the volume is equally likely to contain an Ar atom but no cell can hold more than one Ar atom. Combinatorial arithmetic can determine how many total combinations of Ar placements within the cells there are; and how many combinations have no Ar atoms touching nitromethane (Fig. 9(a)), one Ar atom touching nitromethane (Fig. 9(b)), two Ar atoms touching nitromethane (Fig. 9(c)), etc. This leads to an analytic density-dependent distribution of discrete collision events involving multiple Ar atoms for the *finite* volume system from which the limit of *infinite* volume can be obtained in straightforward fashion. Within the context of the hard-sphere approximation, consider a snapshot of the locations of the Ar atoms with respect to nitromethane at the same given time for each of the 1000 trajectories comprising the ensemble at a given density. For the given time, this would produce an album of 1000 pictures. The fraction of pictures in the album where one, two, three, or more Ar atoms are near nitromethane should be approximated by this combinatorial model. In what follows, the mathematics of this model will be outlined and the parameters necessary to apply it to the simulations will be discussed. The remainder of the section will then explore the dynamical implications of the resulting density-dependent distributions.

Let N be the number of Ar-size cells outside of nitromethane in a large but finite volume that encloses the nitromethane. Let K be the number of those cells that "touch" nitromethane. Let M be the number of Ar atoms. Let V_{Ar} be the volume of one Ar atom, that is, the volume of one cell. If ρ is the number density of Ar atoms in the particular simulation under consideration, then

$$M = \rho V_{Ar} N. \tag{5}$$

The total number of combinations of M atoms in N cells is

$$\text{total combinations} = \frac{N!}{M!(N-M)!}. \tag{6}$$

The total number of combinations of L atoms in K cells and M-L atoms in N-K cells is

$$L \text{ restricted combinations} = \frac{K!}{L!(K-L)!}\frac{(N-K)!}{(M-L)!(N-K-M+L)!}. \tag{7}$$

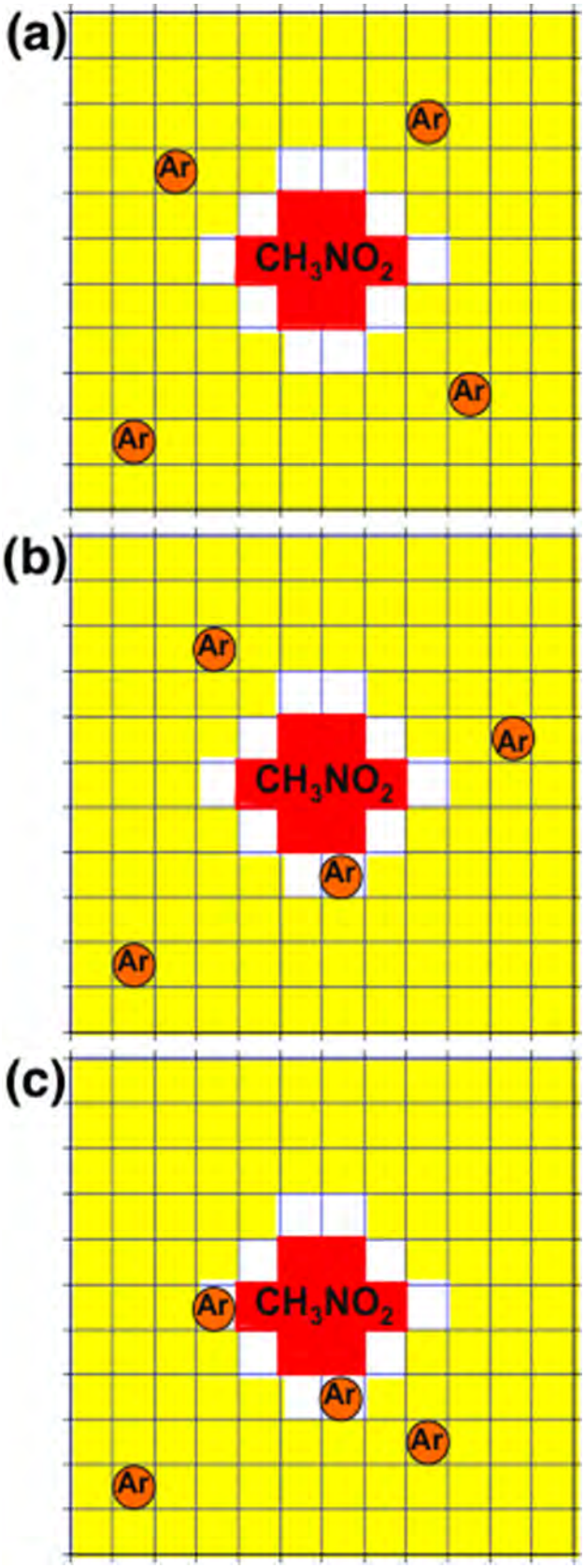

FIG. 9. 2D schematic of three combinations in the combinatorial model for molecule/multi-Ar collisions. White squares "touch" red CH_3NO_2.

In the limit of infinite N

$$\lim_{N\to\infty}\frac{(N-K)!}{(M-L)!(N-K-M+L)!} = (\rho V_{Ar})^L(1-\rho V_{Ar})^{K-L}\frac{N!}{M!(N-M)!}. \tag{8}$$

Let $P(L)$ be the normalized probability of having L atoms in K cells, that is, the ratio of Eq. (8) to Eq. (6)

$$P(L)=\frac{K!}{L!(K-L)!}(\rho V_{Ar})^L(1-\rho V_{Ar})^{K-L} \quad L=[0,1,\ldots,K]. \tag{9}$$

Inspection of this result shows that each $P(L)$ matches a term in the binomial expansion of $(\rho V_{Ar}+1-\rho V_{Ar})^K$, which of course is 1, confirming a normalized probability.

To evaluate $P(L)$ in Eq. (9), V_{Ar} and K must be determined. As discussed in Sec. III B, from the Ar-Ar potential, the hard-sphere radius of Ar is 1.675 Å. V_{Ar} is the volume of the sphere with this radius and K is the maximum number of Ar atoms that can touch the surface of the nitromethane molecule, which has radius $R_{CH_3NO_2}$. This can be approximated by the surface area of a sphere of radius $R_{CH_3NO_2}+R_{Ar}$ divided by the cross-sectional area of Ar. Because a two dimensional array of circles that touch one another have open area in between them, the Ar circular cross-sectional area cannot completely cover the area of the sphere. In this context, a more appropriate estimate of the cross-sectional area of Ar is to treat Ar as a square with edge length $2R_{Ar}$. The result is

$$K=\pi\left(1+\frac{R_{CH_3NO_2}}{R_{Ar}}\right)^2. \tag{10}$$

For $R_{CH_3NO_2}$, a value of 2.2 Å is appropriate based on the equilibrium geometry of nitromethane.[45] Given the values of R_{Ar} and $R_{CH_3NO_2}$, both V_{Ar} and K can be determined, which in turn finalizes for nitromethane/Ar the $P(L)$ distribution once the density ρ is specified.

To understand the dynamical implications of this distribution, consider the simplified relationship between a rate constant k and its scattering cross section σ at low densities

$$k=\rho\sigma v, \tag{11}$$

where v is the averaged thermal relative velocity. In this equation, σ is the *effective* cross section that makes σv equivalent to the integration of the actual collision-energy-dependent cross section over the Boltzmann thermal velocity distribution. Equation (11) expresses the direct proportionality between k_i and ρ at low densities. However, this equation presumes that there is only one dynamical process, namely, the collision of one bath-gas atom with one target molecule.

In Eq. (11), ρv is a flux of atoms, that is, it is the number of atoms per unit time per unit area passing through an arbitrary plane in space. Using $P(L)$, this flux can be decomposed into fluxes for different processes, each one of which can, in principle, have its own cross section. Because $P(L)$ involves L atoms, the density can be decomposed by

$$\rho=\rho\sum_{L=1}^{K}\frac{LP(L)}{\sum_{L=1}^{K}LP(L)}\equiv\rho\sum_{L=1}^{K}P_\rho(L)\equiv\sum_{L=1}^{K}\rho_L, \tag{12}$$

where $P_\rho(L)$ is normalized to unity and ρ_L is the number of atoms per unit volume in a collision event involving L bath atoms and the molecule simultaneously. This decomposition leads

$$\rho v\sigma\to\sum_{L=1}^{K}\rho_L v\sigma_L=\sum_{L=1}^{K}P_\rho(L)\rho v\sigma_L. \tag{13}$$

Here, σ_L is the cross section per atom involved in the collision event and therefore the overall cross section for the process is $L\sigma_L$. This follows from the fact that ρ_L is atom-based while the cross section is for a flux in units of L atoms. Figure 10 shows $P_\rho(L)$ for the eight densities studied. As the density increases, the distribution shifts to multiple Ar collision events.

The fit to k_i in Fig. 7 is a least-squares fit of $v\sigma_L$ in Eq. (13) under the simplification that $v\sigma_L=v\sigma_2$ for all $L\geq 2$. This leaves Eq. (13) with only two adjustable parameters: $v\sigma_1$ and $v\sigma_2$. The resulting fit is quite good, with an rms error of $5.3\times10^{-5}\,\text{ps}^{-1}$ for an average k_i value of $2.1\times10^{-3}\,\text{ps}^{-1}$. While, in principle, more adjustable parameters can be used, adding more of them will not materially improve the fit and indeed, for a sufficiently large number, some of them will optimize to aphysical negative values. The two-parameter fit has a qualitative feature consistent with the k_i reported in Table I at higher densities, as can be seen from the following rearrangement of Eq. (13):

$$\rho v\sigma\to P_\rho(1)\rho v(\sigma_1-\sigma_2)+\sum_{L=1}^{K}P_\rho(L)\rho v\sigma_2 = P_\rho(1)\rho v(\sigma_1-\sigma_2)+\rho v\sigma_2. \tag{14}$$

Specifically, as $P_\rho(1)$ becomes small at higher densities, k_i becomes proportional to density with slope $v\sigma_2$. As $P_\rho(1)$

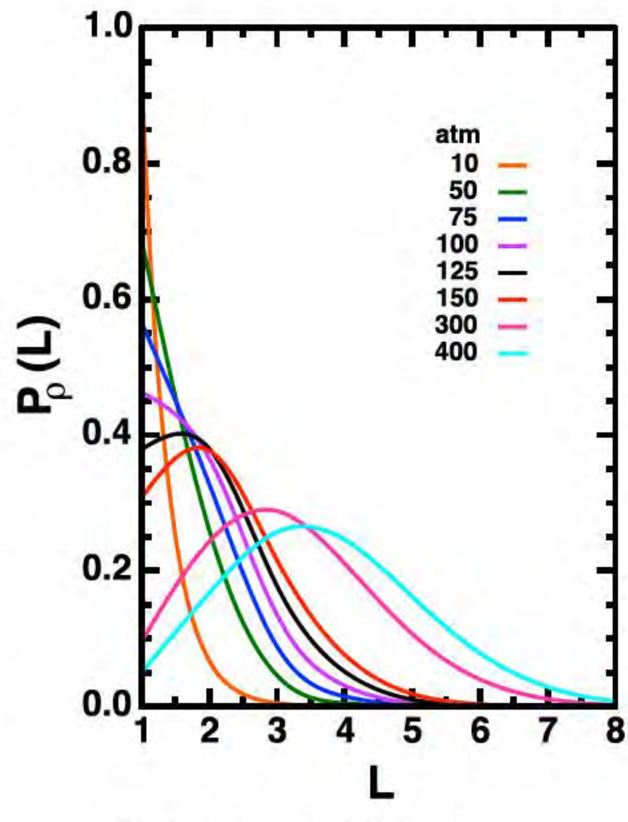

FIG. 10. $P_\rho(L)$ versus L for different densities.

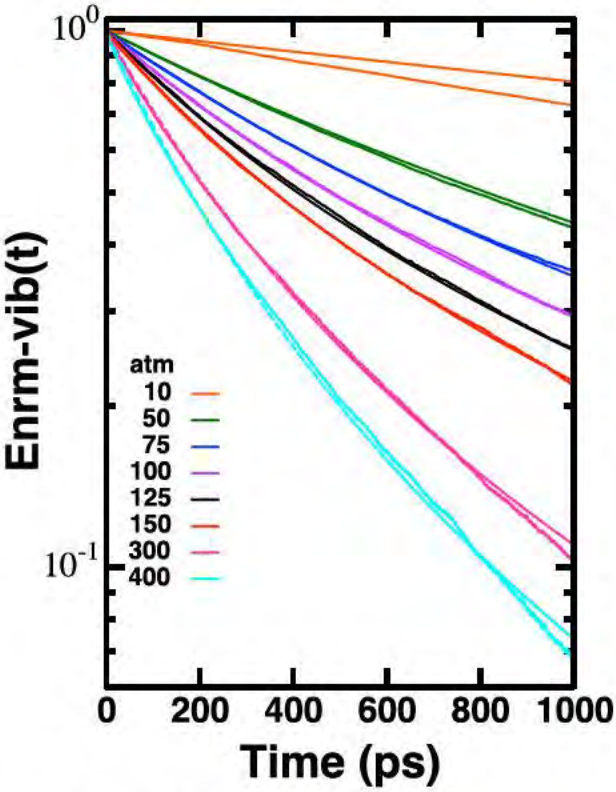

FIG. 11. Same as in Fig. 2 only with fit parameter values determined from their density-dependent functions.

nears unity at low densities, k_i becomes proportional to density with slope $v\sigma_1$. This implies that at higher pressures, k_i does not continuously roll-off from an extrapolation from the limiting low-density results. There is some evidence of this at the highest energies (Fig. 7).

One check of the adequacy of the fitted functions of m and k_i as functions of density is to use the fitted values to reproduce the decay curves in Fig. 2. In Fig. 11, the fits of m and k_i for vibrational relaxation as functions of density, as shown in Figs. 6 and 7, are used to evaluate the LS form of the decay curve in comparison to the trajectory-computed values. In every case, except 10 atm, the parameter functions of density result in quite satisfactory fits to the trajectory data. For 10 atm, the fitted decay is simply too slow. This is a reflection of the fact that in Fig. 7, the largest relative fitting error for k_i occurs at the lowest density (corresponding to 10 atm). As discussed earlier (see Sec. III B), the k_i value in Table I for that density is more representative of a global fitting parameter than of the initial decay rate. The actual initial rate is noticeably lower and is represented by the open circle in Fig. 7. This lower value of k_i is noticeably closer to the fitted value but is still on the high side. For the 10 atm k_i value in Table I, a satisfactory relative error can only be achieved by using more adjustable parameters ($v\sigma_L$); however, some of the optimized values are negative and therefore aphysical. The results for k_i at low pressures will require further studies and a better understanding of the global features of the decay curves.

The optimal values of $v\sigma_1$ and $v\sigma_2$ are 0.98 and 0.45, respectively. For $L \geq 2$, the second number must be multiplied by L to get the correct cross section, that is, $v\sigma_L = Lv\sigma_2$. The optimized values mean that $\sigma_2 \approx \sigma_1$ but $\sigma_{L>2} > \sigma_1$; one would generally expect that collision events involving multiple Ar atoms simultaneously would more rapidly relax a molecule than would a collision event involving only one Ar atom. However, these optimized values also mean that $L\sigma_1 > \sigma_L$ for all $L > 1$. In other words, the multi-collider cross sections are generally larger than the single-collider cross section but *not* L times larger. This makes collision events involving more than one Ar less efficient than L separate collision events with one Ar. This loss in efficiency makes k_i undershoot at high densities the extrapolation from its limiting form at small densities. This undershoot is seen in Fig. 7 to occur at pressures starting at ~100 atm. A plausible physical reason for this loss of efficiency is that multiple Ar atoms involved in a collision expands the number of degrees of freedom that can absorb the collision energy, leading to a "protection" of the target molecule by "boiling off" other Ar atoms involved in the collision. This idea was used by Schwarzer *et al.*[14] in an explanation of azulene/He,Xe relaxation measurements.

The general success of the density-dependent fits of m and k_i in representing the computed vibrational decay curves at all the higher densities motivates an extrapolation of the fit up to solid-state densities. The accuracy of this extrapolation can be affected by the simple, statistical nature of the combinatorial model of Eq. (14) that renders all dynamics into two cross-section parameters adjusted to the lower density results of the simulations. Nonetheless, the extrapolation is instructive and is shown in Fig. 12. The solid-state density cutoff depicted by the dashed vertical line in the figure is the packed-hard-sphere limit discussed in Sec. III B. The pressures needed to condense Ar gas at 300 K are very much larger than the pressures studies here. However, from the density perspective,

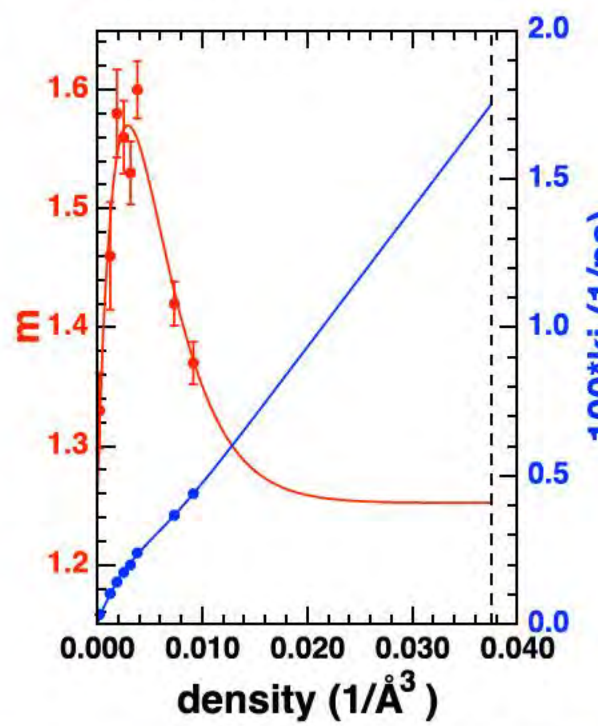

FIG. 12. The vibrational m and k_i functions of density in Figs. 6 and 7 extended to solid-state densities. The dashed vertical line corresponds to the nominal solid-state density. The solid curves are the fits discussed in the text.

the highest density simulated in the present study is already 25% of the way to the solid-state cutoff. As seen in Fig. 12, both the m and k_i functions behave smoothly with density up to the solid-state limit. The recovery of linear dependence of the initial rate k_i with density at high density, as discussed in connection with Eq. (13) and hinted at in Fig. 7, is clearly evident in the initial rate fit in the approach to solid-state density. Because m is substantially larger than unity over the whole interval of densities studied, the initial rate k_i in Fig. 12 is the maximum rate achieved during the decay. As more energy drains out of the molecule, the rate of subsequent decay will slow down.

For rotational relaxation, as shown in Fig. 8, the rate of decay slows down as rotational energy drains out of the molecule. However, unlike vibrational decay, the k_i for rotational decay is essentially directly proportional to density for the interval of densities studied. Rotational relaxation occurs at longer range than vibrational relaxation because the quantum of energy is so much smaller, such that glancing collisions can be effective. Therefore, one would expect that if simultaneous molecular collisions with multiple Ar atoms are important for vibrational relaxation, then they are also important for rotational relaxation. In this regard, if σ_L were the same for all L, then multi-Ar collisions with nitromethane could occur but the end result would still be direct proportionality to density over the entire density interval examined. Further studies are needed to clarify the differences between rotational and vibrational relaxations.

The above discussion focuses on the extrapolation to the high-density regime of the relaxation in the gas phase. Most previous theoretical studies of vibrational relaxation are in the *low*-density regime of isolated binary collisions and produce ΔE, defined earlier as the average energy lost per collision by the molecule with initial energy E. Unfortunately, even the lowest pressure examined in our study, 10 atm, is still not low enough to unambiguously identify single collision events directly from the trajectories. For example, if one samples the instantaneous vibrational energy of nitromethane every $t_k - t_{k+1} = 50$ fs during a typical 10 atm trajectory over an extended period of time (say 100 ps) and computes the distribution of successive vibrational energy changes, $P(E(t_k) - E(t_{k-1}))$, this will yield a distribution that has an average very near to zero, a standard deviation of ~0.1 kcal/mol, and a few outliers that range to as much as ~1 kcal/mol. A definition of a collision as one that produces a change of "x" times the standard deviation cannot be derived from more rigorous theory and will produce "single" collision properties that are critically dependent on the value of "x."

While the trajectories of our study cannot be used to unambiguously identify single collision events, there are approximate models of Z, the number of collisions per unit time, that are based on the cross sectional area of interaction potentials. Such models are implicitly derived in the context of isolated binary collisions and are directly proportional to the bath gas density. Given a model of Z, then in the low pressure limit of isolated collisions

$$\frac{dE}{dt} = \frac{dn}{dt}\frac{dE}{dn} = Z\Delta E, \tag{15}$$

where n is the isolated collision number from the start of the trajectories. From Eq. (4) for the LS functional form, it is easy to show that

$$\frac{dE}{dt} = -k_i E(0)\left(\frac{E(t)}{E(0)}\right)^m \xrightarrow[t=0]{} -k_i E(0). \tag{16}$$

Combining Eq. (15) with the above equation in the low-pressure limit of isolated collisions leads at $t = 0$ to

$$\Delta E = -\frac{k_i}{Z}E(0). \tag{17}$$

Z is linearly dependent on pressure (or density) and in the low pressure limit k_i is also, making their ratio and consequently ΔE pressure independent. The fit of k_i as a function of density follows from a combinatorial model that used a hard sphere estimation of both Ar and CH_3NO_2. For consistency, the well known hard sphere model can be used for Z

$$Z = \rho(R_{CH3NO2} + R_{Ar})^2\sqrt{\frac{8kT}{\pi\mu}}, \tag{18}$$

where μ is the reduced mass for Ar + CH_3NO_2. Using the fit of k_i and values of $R_{CH_3NO_2}$ and R_{Ar} derived previously, from Eq. (17) the low density limiting value of ΔE_{vib} is −0.18 kcal/mol.

There are a few single-collision theoretical studies using Ar as a bath gas where the molecule is initially excited by amounts similar to that studied here. The most relevant is Lenzer *et al.*[46] who studied rotationally equilibrated C_6H_6 with 68.6 kcal/mol initial vibrational excitation in a 300 K Ar bath and found that $\Delta E_{vib} = -0.094 \pm 0.014$ kcal/mol. The value was found to be quite sensitive to the nature of the interaction potential, which is not well known. Lendvay and Schatz[47] studied rotationally equilibrated SF_6 vibrationally excited to 50 kcal/mol in a 300 K Ar bath and found that $\Delta E_{vib} = -0.06$ kcal/mol. Lendvay *et al.*[48] studied rotationally equilibrated SO_2 vibrationally excited to 57 kcal/mol in a 300 K Ar bath and found that $\Delta E_{vib} = -0.20$ kcal/mol or −0.49 kcal/mol depending on the nature of the potential. All three of these published results involve a fixed initial vibrational excitation and a thermal rotational distribution, whereas the studies here involved a fixed total internal energy maintained by a correlated efficient microcanonical sampling (EMS) vibrational and rotational distributions. Given the differences in systems and initial conditions, our limiting single collision estimate of $\Delta E_{vib} = -0.18$ kcal/mol is not inconsistent with past studies.

V. CONCLUSIONS

Classical molecular dynamics simulations were performed to study the relaxation of nitromethane in an Ar bath as a function of pressure $P = 10$, 50, 75, 100, 125, 150, 300, and 400 atm at 300 K. At the highest pressure, the density of the gas is ~25% of the solid-state density. The molecule was instantaneously excited by statistically distributing 50 kcal/mol among the internal degrees of freedom. At each pressure, 1000 periodic boundary condition trajectories followed nitromethane and 1000 Ar atoms explicitly for 1000 ps, except for 10 atm for which the simulations were extended to 5000 ps. The ensemble-averaged vibrational and rotational energies were calculated as functions of time. The simulations are long enough for a

substantial amount of the vibrational decay, and almost all of the rotational decay, to occur.

The rotational energy undergoes fast decay to ~5% of the original energy. There follows a very slow decay, the origin of which is not yet clear and for which characterization will require further study with improved statistics. The dominant rotational decay and the vibrational decay curves can be satisfactorily fit with the Lendvay-Schatz functional form, Eq. (4).[19] This form has two parameters; one that is sensitive to the initial rate of decay and one that is sensitive to the curvature of the decay curve. All decay curves at all pressures exhibit positive curvature, which implies that the rate of decay decreases as energy drains out of the molecule and is therefore *not* describable by a single-exponential function. The initial rotational relaxation rate is nearly directly proportional to density over the entire interval of density studied. By contrast, the initial vibrational rate is *not* directly proportional to density over that same interval. Rather, with increased density the initial rate falls away from the extrapolation of the limiting low-pressure proportionality to density.

Fits to the two Lendvay-Schatz parameters were independently determined as functions of density over the interval of densities studied. For the initial rate, the functional form arises from a model of the probability of individual nitromethane collision events that involve multiple Ar atoms. This model is based on the combinatorial arithmetic for randomly filling space near the nitromethane molecule with Ar atoms for different bulk densities. The model suggests that at the higher densities studied, collisions involving multiple Ar atoms become the rule rather than the exception. Roll-off of the initial rate from the low-density extrapolation occurs because the cross section for collision events with L Ar atoms grows with L more slowly than L times the cross section for collision events with one Ar atom. The resulting density-dependent function of k_i represents, reasonably well, the individually computed k_i values, with the poorest agreement occurring at the lowest density. Given the density-dependent functions for the two parameters in the Lendvay-Schatz form, all the vibrational decay curves are well represented except at the lowest density for which the decay is somewhat too slow. Extrapolation of the parameter functions gives a prediction of the decay over all densities corresponding to the gas phase.

Further studies are required to

- Characterize the residual rotational decay;
- understand the molecular mechanisms at work for initial vibrational and rotational decays, in part, by testing the combinatorial model for multiple collisions; and
- understand the molecular mechanisms at work that produce positive curvature for vibrational and rotational relaxations.

The studies reported here involve only one temperature and only one kind of initial molecular excitation. A full understanding of the molecular mechanisms involved will require the ability to predict and explain changes in temperature and excitation. What the current study has accomplished is the development of feasible and reliable methods to simulate the relaxation and a framework of analysis that allows appropriate questions to be posed and hopefully answered.

Additional studies of nitromethane are in the planning stages. Similar studies on HO_2 and HO relaxation in Ar are in progress. Preliminary results on HO_2 at $T = 800$ K indicate behavior qualitatively similar to that of nitromethane.

ACKNOWLEDGMENTS

This material is based upon work supported by the U.S. Army Research Office under Grant No. W911NF-09-1-0199 (L.R.R., T.S., and D.T.) and the U.S. Department of Energy, Office of Science, Office of Basic Energy Sciences, Division of Chemical Sciences, U.S. Department of Energy under Contract No. DE-AC02-06CH11357 (A.W.).

[1]Department of Energy workshop report: Basic Research Needs for Clean and Efficient 21st Century Transportation Fuels, and references therein, http://science.energy.gov/~/media/bes/pdf/reports/files/ctf_rpt.pdf, 2006, pp. 95–101.
[2]J. R. Barker and D. M. Golden, Chem. Rev. **103**, 4577 (2003).
[3]D. M. Golden, Chem. Soc. Rev. **37**, 717 (2008).
[4]D. M. Golden and J. R. Barker, Combust. Flame **158**, 602 (2011).
[5]A. W. Jasper and J. A. Miller, J. Phys. Chem. A **115**, 6438 (2011).
[6]Y. Georgievskii, J. A. Miller, M. P. Burke, and S. J. Klippenstein, J. Phys. Chem. A **117**, 12146 (2013).
[7]J. R. Barker, L. M. Yoder, and K. D. King, J. Phys. Chem. A **105**, 796 (2001).
[8](a) Q. Liu, D. K. Havey, and A. S. Mullin, J. Phys. Chem. A **112**, 9509 (2008); (b) K. Sekiguchi, A. Shimojima, and O. Kajimoto, Chem. Phys. Lett. **356**, 84 (2002); (c) D. J. Myers, M. Shigeiwa, M. D. Fayer, and B. J. Cherayil, J. Phys. Chem. B **104**, 2402 (2000).
[9]D. G. Mitchell, A. M. Johnson, J. A. Johnson, K. A. Judd, K. Kim, M. Mayhew, A. L. Powell, and E. T. Sevy, J. Phys. Chem. A **112**, 1157 (2008).
[10]J. E. Dove, H. Hippler, and J. Troe, J. Chem. Phys. **82**, 1907 (1985).
[11]H.-C. Hsu, C.-L. Liu, Y. C. Hsu, and C.-K. Ni, J. Chem. Phys. **129**, 044301 (2008).
[12]J. H. Kiefer, C. Katopodis, S. Santhanam, N. K. Srinivasan, and R. S. Tranter, J. Phys. Chem. A **108**, 2443 (2004); J. H. Kiefer, S. Santhanam, N. K. Srinivasan, R. S. Tranter, S. J. Klippenstein, and M. A. Oehlschlaeger, Proc. Combust. Inst. **30**, 1129 (2005).
[13]C. G. Elles and F. F. Crim, Annu. Rev. Phys. Chem. **57**, 273 (2006).
[14]D. Schwarzer, J. Troe, M. Votsmeier, and M. Zerezke, J. Chem. Phys. **105**, 3121 (1996).
[15]D. Schwarzer, J. Troe, and M. Zerezke, J. Chem. Phys. **107**, 8380 (1997).
[16]L. Ming, T. D. Sewell, and S. Nordholm, Chem. Phys. **199**, 83 (1995).
[17]A. W. Jasper and J. A. Miller, J. Phys. Chem. A **113**, 5612 (2009).
[18]J. R. Barker and R. E. Weston, Jr., J. Phys. Chem. A **114**, 10619 (2010).
[19]G. Lendvay and G. C. Schatz, J. Phys. Chem. **95**, 8748 (1991).
[20]C. Heidelbach, I. I. Fedchenia, D. Schwarzer, and J. Schroeder, J. Chem. Phys. **108**, 10152 (1998).
[21]C. Heidelbach, I. I. Fedchenia, D. Schwarzer, and J. Schroeder, Chem. Phys. Lett. **291**, 333 (1998).
[22]S. Li and W. H. Thompson, J. Phys. Chem. A **107**, 8696 (2003).
[23]A. K. Paul, S. C. Kohale, S. Pratihar, R. Sun, S. W. North, and W. L. Hase, J. Chem. Phys. **140**, 194103 (2014).
[24]Reference 23 does not comment on or display the pressure dependence of their computed relaxation rates. However, plots of the rates listed in the paper exhibit a roll-off of proportionality with pressure at high pressures.
[25]D. C. Sorescu, B. M. Rice, and D. L. Thompson, J. Phys. Chem. B **104**, 8406 (2000), There were two typographical errors in the original presentation of this force field: (1) Eq. (6) for the harmonic three-center covalent bending angle should not contain the factor of 1/2 that appears there and (2) the energy coefficient V_ϕ for the N_2–O_4–O_3–C_1 improper dihedral angle interaction in Table I is exactly twice as large as it should be. Both of these typographical errors were fixed in Ref. 27. Another feature of the SRT force field model for nitromethane that should be appreciated is that it does not possess permutation symmetry with respect to hydrogen atom exchange, with the consequence that it is important for a correct implementation of the potential to number the atoms in accord with the convention shown in Fig. 1 of this reference (or Fig. 1(a) of Ref. 27).
[26]*CRC Handbook of Chemistry and Physics*, 92nd ed., edited by W. M. Haynes (CRC Press, Boca Raton, FL, 2011), p. 4-121.
[27]P. M. Agrawal, B. M. Rice, and D. L. Thompson, J. Chem. Phys. **119**, 9617 (2003).

[28]E. A. Colbourn and A. E. Douglas, J. Chem. Phys. **65**, 1741 (1976).
[29]D. C. Sorescu, B. M. Rice, and D. L. Thompson, J. Phys. Chem. B **101**, 798 (1997), Note that the parameter $B'_{\beta\beta}$ listed in this reference is the inverse of what is required in Eqs. (1) and (2) in the present paper because of a redefinition of the exponential term in the potential.
[30]G. Z. Whitten and B. S. Rabinovitch, J. Chem. Phys. **38**, 2466 (1963); *ibid.* **41**, 1883 (1964).
[31]The probability $P(n)$ of the nth harmonic quantum state of frequency ν being occupied at a temperature T is $e^{-n\beta}(1-e^{-\beta})$ where $\beta = \frac{h\nu}{kT}$. Then the thermal energy above the zero point energy is $\frac{\sum_{n=0}^{\infty}(n+.5)h\nu P(n) - .5h\nu = h\nu\sum_{n=0}^{\infty} nP(n) = h\nu e^{-\beta}}{1-e^{-\beta}}$. This has the correct limits of kT as $T \to \infty$ and 0 as $T \to 0$.
[32]S. Plimpton, J. Comput. Phys. **117**, 1 (1995).
[33]A customized version based on the code GENDYN was used to calculate initial conditions for the excited molecule, http://www.chem.missouri.edu/Thompson/research/gendyn.htm.
[34]The Markov walk was performed using a version of EMS:, G. Nyman, K. Rynefors, and L. Holmlid, J. Chem. Phys. **88**, 3571 (1988); G. Nyman, S. Nordholm, and H. W. Schranz, ibid. **93**, 6767 (1990); H. W. Schranz, S. Nordholm, and G. Nyman, ibid. **94**, 1487 (1991).
[35]W. G. Hoover, Phys. Rev. A **31**, 1695 (1985).
[36]D. E. Woon, Chem. Phys. Lett. **204**, 29 (1993).
[37]T. Pfleiderer, I. Waldner, H. Bertagnolli, K. Todheide, B. Kirchner, H. Huber, and H. E. Fischer, J. Chem. Phys. **111**, 2641 (1999).
[38]Consider the Taylor series expansion of $(1+(1-m)k_it)^{\frac{1}{1-m}}$ as a function of k_it. The first derivative takes the form $-(1+(1-m)k_it)^{\frac{m}{1-m}}$ and the second derivative takes the form $(1+(1-m)k_it)^{\frac{2m-1}{1-m}}$. Given that unity raised to any power including infinity is still unity, these two derivatives evaluated exactly at $m = 1$ return -1 and $+1$, respectively. In fact, in the limit of $m = 1$, all derivatives in the Taylor series expansion are $+1$ if it is an even derivative and -1 if it is an odd derivative. Using the derivatives in the $m = 1$ limit, the Taylor series can be formally written as a function of k_it and that expansion is identical to the Taylor series expansion of e^{-k_it}.
[39]B. Efron, SIAM Rev. **21**, 460 (1979); P. Diaconis and B. Efron, Sci. Am. **248**, 116 (1983).
[40]T. C. Hales, "An overview of the Kepler conjecture," e-print arXiv:math/9811071v2(1998).
[41]D. G. Henshaw, Phys. Rev. **111**, 1470 (1958).
[42]O. G. Peterson, D. N. Batchelder, and R. O. Simmons, Phys. Rev. **150**, 703 (1966).
[43]The system volumes at the respective pressures were re-determined for the modified potential using the NPT simulation protocol described in Sec. II B.
[44]R. N. Schwartz, Z. I. Slawsky, and K. F. Herzfeld, J. Chem. Phys. **20**, 1591 (1952).
[45]From the exp-6 parameters, hard-sphere diameters for the pairwise potentials are 3.35 Å for Ar–Ar, 3.18 Å for Ar–O, and 3.10 Å for Ar–H. From this, the radius of Ar is 3.35 Å/2 = 1.675 Å. From this and using the equilibrium N–O and C–H distances in nitromethane, the distance at which nitromethane is just touching Ar along the N–O bond vector is 2.735 Å and along the C–H bond vector is 2.515 Å. Given the equilibrium bond angles, the projection of each of these distances on the axis through the C–N bond is 1.244 Å for N–O and 0.759 Å for C–H. Given the C–N bond length, this makes the length of nitromethane along this axis 3.503 Å or a radius of 1.770 Å. The projection perpendicular to this axis of the vector along the N–O (C–H) bond gives a radius of 2.435 Å (2.393 Å). The average of these three estimates of the nitromethane hard-sphere radius is 2.2 Å
[46]T. Lenzer, K. Luther, J. Troe, R. G. Gilbert, and K. F. Lim, J. Chem. Phys. **103**, 626 (1995).
[47]G. Lendvay and G. C. Schatz, J. Chem. Phys. **98**, 1034 (1993).
[48]G. Lendvay, G. C. Schatz, and L. B. Harding, Faraday Discuss. **102**, 389 (1995).